International Journal of Nanomedicine

Dovepress
open access to scientific and medical research

Open Access Full Text Article

ORIGINAL RESEARCH

Designing Mesoporous Prussian Blue@zinc Phosphate Nanoparticles with Hierarchical Pores for Varisized Guest Delivery and Photothermally-Augmented Chemo-Starvation Therapy

Yuan Yuan[1,*], Mingyi Hou[2,*], Xiaoning Song[1], Xintao Yao[1], Xuerui Wang[1], Xiangjun Chen[2], Shengnan Li[1]

[1]School of Chemical Engineering and Technology, Hebei University of Technology, Tianjin, 300401, People's Republic of China; [2]School of Pharmacy, Shandong New Drug Loading & Release Technology and Preparation Engineering Laboratory, Binzhou Medical University, Yantai, 264003, People's Republic of China

*These authors contributed equally to this work

Correspondence: Shengnan Li; Xiaoning Song, School of Chemical Engineering and Technology, Hebei University of Technology, Xiping Road, Tianjin, 300401, People's Republic of China, Email lisn027@hebut.edu.cn; songxn123@hebut.edu.cn

Background: With the rapid development of nanotechnology, constructing a multifunctional nanoplatform that can deliver various therapeutic agents in different departments and respond to endogenous/exogenous stimuli for multimodal synergistic cancer therapy remains a major challenge to address the inherent limitations of chemotherapy.

Methods: Herein, we synthesized hollow mesoporous Prussian Blue@zinc phosphate nanoparticles to load glucose oxidase (GOx) and DOX (designed as HMPB-GOx@ZnP-DOX NPs) in the non-identical pore structures of their HMPB core and ZnP shell, respectively, for photothermally augmented chemo-starvation therapy.

Results: The ZnP shell coated on the HMPB core, in addition to providing space to load DOX for chemotherapy, could also serve as a gatekeeper to protect GOx from premature leakage and inactivation before reaching the tumor site because of its degradation characteristics under mild acidic conditions. Moreover, the loaded GOx can initiate starvation therapy by catalyzing glucose oxidation while causing an upgradation of acidity and H_2O_2 levels, which can also be used as forceful endogenous stimuli to trigger smart delivery systems for therapeutic applications. The decrease in pH can improve the pH-sensitivity of drug release, and O_2 can be supplied by decomposing H_2O_2 through the catalase-like activity of HMPBs, which is beneficial for relieving the adverse conditions of anti-tumor activity. In addition, the inner HMPB also acts as a photothermal agent for photothermal therapy and the generated hyperthermia upon laser irradiation can serve as an external stimulus to further promote drug release and enzymatic activities of GOx, thereby enabling a synergetic photothermally enhanced chemo-starvation therapy effect. Importantly, these results indicate that HMPB-GOx@ZnP-DOX NPs can effectively inhibit tumor growth by 80.31% and exhibit no obvious systemic toxicity in mice.

Conclusion: HMPB-GOx@ZnP-DOX NPs can be employed as potential theranostic agents that incorporate multiple therapeutic modes to efficiently inhibit tumors.

Keywords: Prussian Blue, glucose oxidase, co-delivery system, photothermal therapy, chemotherapy

Introduction

Cancer is a malignant disease that causes millions of deaths each year.[1] Owing to its toxic effects on healthy organs and drug resistance, chemotherapy as the primary treatment method has been significantly restricted in clinical application.[2–5] Especially, doxorubicin (DOX) have been the mainstay of cancer therapy since long, which is a water-soluble and photosensitive chemotherapeutic drug that isolated from Streptomyces peucetius var. caesius.[6–10] With the rapid

Received: 15 February 2024
Accepted: 18 June 2024
Published: 8 July 2024

Graphical Abstract

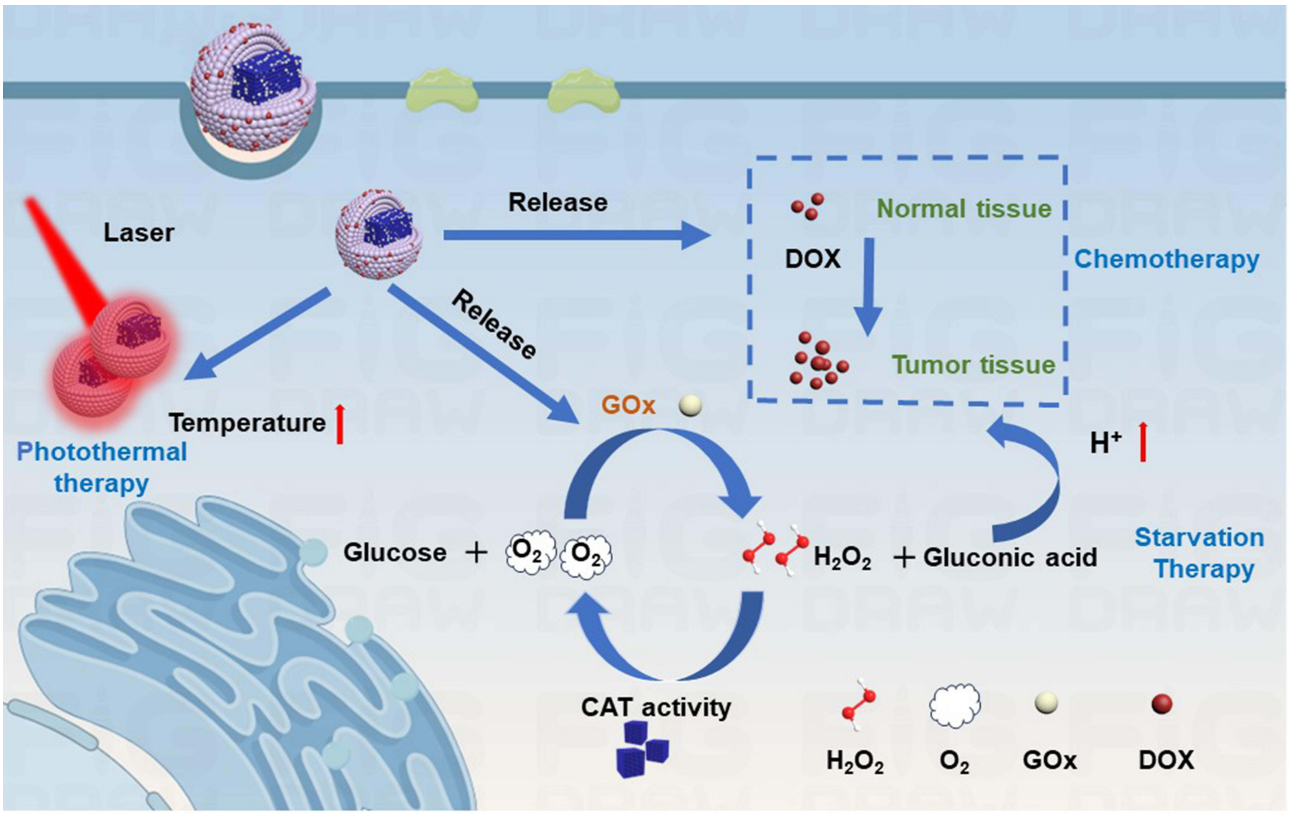

development of nanotechnology, designing novel nanoscale delivery systems that can be effectively enriched at tumor sites and exhibit controlled drug release under endogenous or exogenous stimuli has become more focused on addressing the inherent limitations of chemotherapy.[11–13] In addition, integrating multiple advanced therapeutic modes with chemotherapy has a higher probability of achieving better therapeutic outcomes than monotherapy.[14–16]

Starvation therapy is widely considered a fascinating therapeutic strategy to induce cancer cell death by curbing the energy supply for tumors.[17,18] Glucose oxidase (GOx) is frequently employed as a starvation agent through competitive consumption of nutrients because it can effectively convert glucose into gluconic acid and hydrogen peroxide (H_2O_2) in the presence of oxygen (O_2).[19] Notably, the reduced pH and elevated H_2O_2 levels caused by GOx-catalyzed reaction products can serve as forceful endogenous stimuli to trigger smart delivery systems for therapeutic applications.[20] GOx has been utilized to improve the pH sensitivity of drug release to boost synergistic chemotherapy.[21] Meanwhile, elevated H_2O_2 levels can act as a reactant for enzymatic decomposition into O_2, thereby upgrading the effectiveness of chemotherapy and GOx-mediated starvation therapy limited by tumor hypoxia.[22] It can be seen that constructing GOx/chemical drug co-delivery systems can not only achieve a simple combination of chemotherapy and starvation therapy, but can also utilize its products to form appropriate endogenous stimuli to upgrade the collaborative effect. However, problems with using an overdose of the drug and controlling drug release may cause unexpected damage to normal tissues. Therefore, designing smart drug co-delivery platforms with endogenous stimulus-responsive ability that can also be activated by exogenous stimuli still needs to focus on further reducing systemic toxicity and amplifying the therapeutic effect of chemotherapy and starvation therapy.

Photothermal therapy (PTT) is a typical minimally invasive therapeutic technique that is triggered by near-infrared (NIR) light as an excellent external stimulus to kill tumors through thermal ablation.[23–27] Moreover, the generated local hyperthermia can enhance the enzymatic activities of GOx while also promoting the internalization of nanoagents by

disrupting the integrity and permeability of tumor cell membranes and expediting drug release.[28–32] Thus, the integration of GOx/chemical drug co-administration and photothermal conversion ability is a credible approach to maximize synergistic therapeutic effect.[33,34] Notably, hollow mesoporous Prussian Blue nanoparticles (HMPB NPs) can serve as biologically friendly photothermal agents and carrier substrates for GOx, owing to their high absorption coefficient in the NIR region and suitable pore size.[35] Moreover, it can catalyze the decomposition of H_2O_2 in tumors to achieve rapid reoxygenation owing to its catalase-like activity, which may help to avoid the problems associated with tumor hypoxia. To date, research on HMPB NP-based GOx or drug delivery systems for combined therapy has made some progress.[36,37] However, to avoid mutual influence between therapeutic agents with diverse physicochemical properties, administration into discrete departments of a single delivery system based on HMPB NPs remains a great challenge. In particular, it is difficult to construct co-delivery nanoplatforms with hierarchical porous structures to load varisized guests based on widely used carriers, such as core-shell and hollow-structured NPs, which generally possess symmetrical concentric structures and uniform mesopores but do not have separate storage space.[38] Thus, it is necessary to develop an HMPB NP-based nanoplatform via a mild route to achieve the co-delivery of two therapeutic agents with different sizes and properties in discrete compartment nanostructures for photothermally augmented chemo-starvation therapy.

In this study, we synthesized HMPB@zinc phosphate core-shell NPs with non-identical pore sizes in the core and shell regions for the co-delivery of GOx and DOX (HMPB-GOx@ZnP-DOX NPs) to realize photothermally augmented chemo-starvation therapy. In this system, the central cavity of the HMPB core was utilized to load macromolecular GOx, and the surface of the GOx-loaded HMPB was subsequently coated with ZnP, which possesses smaller mesopores to load DOX, and can protect GOx from premature leakage and degradation when exposed to biological environments.[39] After successful endocytosis, the ZnP shell decomposed under slightly acidic conditions for efficient release of DOX and GOx. Moreover, HMPB-catalyzed H_2O_2 decomposition can replenish oxygen to relieve adverse conditions of anti-tumor. In addition, upon NIR irradiation, HMPB can cause a temperature increase at tumor sites via its good photothermal conversion ability, which contributes to enhancing the drug release rate and enzymatic activities for amplified chemotherapy and starvation therapy. Taken together, the above multifunctional nanoplatforms can not only realize the delivery of DOX and GOx in separate storage spaces but also achieve photothermally augmented chemo-starvation therapy to effectively suppress tumor growth.

Experimental Section

Synthesis of Prussian Blue (PB) NPs

PVP (3.003 g) and $K_3[Fe(CN)_6]$ (0.132 g) were added into 40 mL of HCl (0.01 M) with constant stirring. The solution became transparent and was heated in an oven at 80 °C for 20 h. After the solution cooled, the products were collected by centrifugation and washed several times with deionized (DI) water.

Preparation of HMPB NPs

PB NPs (20 mg) and PVP (100 mg) were dissolved in Teflon with HCl (1.0 M, 20 mL) and the solution was heated at 140 °C for 4 h in an oven. The products were collected by centrifugation and washed several times with DI water. The final product was re-dispersed in DI water (5 mL) for further use.

Preparation of HMPB-GOx NPs

The HMPB NPs (2 mg) was stirred with a GOx aqueous solution (1 mL, 2 mg mL^{-1}) in the dark for 24 h. The HMPB-GOx products were collected by centrifugation and dispersed in 5 mL DI water for subsequent experiments.

Preparation of HMPB-GOx@ZnP NPs and HMPB-GOx@ZnP-DOX NPs

Briefly, to coat the surface of HMPB-GOx with ZnP for preparing HMPB-GOx@ZnP NPs, zinc oxide (ZnO, 5 mg) and polyacrylic acid (PAA) solution (230 μL, 0.2 g mL^{-1}) were mixed in DI water (20 mL) and stirred until the solution became transparent, which called PAA-Zn solution. Then 2.7 mL of HMPB-GOx NPs was placed to the PAA-Zn aqueous solution. After stirring for 2 h, isopropanol (IPA, 40 mL) was added dropwise. Then, 20 mg of $NH_4H_2PO_4$ was

added to react overnight to form the HMPB-GOx@ZnP NPs. To load DOX into the ZnP shell, DOX was mixed with an equal mass of the HMPB-GOx@ZnP NPs and stirred for 24 h in the dark. The final HMPB-GOx@ZnP-DOX NPs were separated by centrifugation and washed twice to remove the unloaded DOX. All supernatants were collected to measure the encapsulation rate and loading content. The HMPB@ZnP NPs synthesis method was consistent with that described above, except that it was not loaded with GOx or DOX.

Photothermal Performance Study

First, HMPB-GOx@ZnP-DOX NPs aqueous solutions (300 μL) at different concentrations (50, 100, 150 and 200 μg mL^{-1}) were irradiated with an NIR laser (808 nm, 1.0 W cm^{-2}) for 5 min, and the temperature of the solutions was recorded. Then, the photothermal effect of HMPB-GOx@ZnP-DOX solution (300 μg mL^{-1}) under different intensities of NIR laser (0.25, 0.5, 1.0 and 1.5 W cm^{-2}) was also studied. In addition, the photothermal stability of the HMPB-GOx@ZnP-DOX NPs was determined using four on/off laser cycles of irradiation for 10 min. The distance from the laser to the NPs solution is 10 cm. The photothermal conversion efficiency of HMPB-GOx@ZnP-DOX NPs was calculated based on a previous research.[40]

DOX Releasing Property

First, the encapsulation rate and drug loading content of the HMPB-GOx@ZnP-DOX NPs were calculated according to the standard UV-vis curve of DOX. Equal masses of HMPB-GOx@ZnP-DOX NPs were dispersed in 30 mL of PBS solution (pH 7.4, 5.3) at 37°C. At designated time intervals, 2 mL of the samples was removed and measured using a UV-vis spectrophotometer to determine the amount of released DOX. To study whether temperature can effectively increase drug release, the same amount of HMPB-GOx@ZnP-DOX NPs was irradiated by an 808 nm laser (1 W/cm^2) for 5 min at selected times at pH 5.3, and the follow-up operation was the same as above.

Enzyme Activity Assay of HMPB-GOx@ZnP-DOX NPs

GOx can catalyze the oxidation of glucose to H_2O_2 and gluconic acid in the presence of oxygen, so the enzyme activity can be investigated by detecting the change of H_2O_2 production and pH value. The production of H_2O_2 was assessed using $TiOSO_4$, which can react with H_2O_2 to form yellow substance with an obvious absorption peak at 405 nm. Briefly, glucose (10 mM) and HMPB-GOx@ZnP-DOX NPs (100 mg mL^{-1}) were first mixed at 37 °C. Then, 0.30 mL of the supernatant after centrifugation was mixed with 2.70 mL of $TiOSO_4$ solution (300 mg $TiOSO_4$ was dissolved in 30 mL of water containing 5 mL of H_2SO_4), and the H_2O_2 level was measured by UV-Vis spectrophotometer. Pure glucose, glucose + free GOx and glucose + HMPB-GOx@ZnP-DOX NPs were dissolved in deionized water and the corresponding pH values were measured using a pH meter. To test the regulation effect of NIR irradiation on enzymatic activity, HMPB-GOx@ZnP-DOX NPs were mixed with glucose (6 mg mL^{-1}) and irradiated under an 808 nm laser with power densities of 0, 0.25, 0.5, 1.0 and 1.5 W cm^{-2} for 5 min, and then the concentration of H_2O_2 was measured according to the above methods.

Oxygen Production Capacity

To evaluate the O_2 production capacity, HMPB@ZnP NPs and HMPB-GOx@ZnP-DOX NPs (200 μg mL^{-1}) were incubated with H_2O_2 solution. The O_2 concentration in the aqueous solution was measured using a dissolved-O_2 meter.

In vitro Cellular Uptake

To demonstrate the cellular uptake of the HMPB-GOx@ZnP-DOX NPs, HepG-2 cells (purchase from BeNa Culture Collection, Henan, China) were seeded in 24-well plates and incubated overnight. The cells were then incubated with a culture medium containing HMPB-GOx@ZnP-DOX NPs (30 μg mL^{-1}) for 3 h. After the cells were washed three times with PBS, they were stained with 4',6-diamidino-2-phenylindole (DAPI) for 15 min and observed by confocal laser scanning microscopy (CLSM). Cells treated with HMPB-GOx@ZnP-DOX NPs at different times were collected by digestion, and the intrinsic specific red fluorescence of DOX in the cells was measured by quantitative flow cytometric analysis to examine cellular uptake.

Detection of Intracellular ATP Level

To explore HMPB-GOx@ZnP-DOX NPs for starvation therapy in vitro, an ATP test was carried out.

After the HepG-2 cells were seeded in a 12-well plate for 24 h, the cells were replaced with fresh cell culture media, free GOx, HMPB@ZnP NPs and HMPB-GOx@ZnP-DOX NPs (GOx: 0.5 μg mL^{-1}) and cultured for varying point of time (0 h, 2 h, 4 h, 6 h). Then, the cells were collected and lysed, and the obtained supernatant was used to evaluate the ATP level by an ATP assay kit.

Cytotoxicity of HMPB-GOx@ZnP-DOX NPs

A 3-(4,5-Dimethylthiazol-2-yl)-2,5-diphenyltetrazolium bromide (MTT) assay was used to evaluate the cytotoxicity of HMPB-GOx@ZnP-DOX NPs in HepG-2 cells. The cells were divided into five groups: (1) control, (2) HMPB@ZnP NPs, (3) HMPB-GOx@ZnP NPs, (4) HMPB-GOx@ZnP-DOX NPs, and (5) HMPB-GOx@ZnP-DOX NPs + laser. Cells that required laser treatment were irradiated with an 808 nm laser for 5 min. After 24 h of cell culture, MTT (10 μL) was added and incubated for 4 h. Finally, 100 μL of DMSO solution was added to each well and cell viability was measured using a microplate reader. In addition, cells subjected to different treatments were stained with calcein-AM and propidium iodide (PI) for 30 min. After washing with PBS, cells were subjected to fluorescence imaging. After various treatments, the cells were washed and were measured by the standard method of flow cytometry.

In vivo Anti-Tumor Efficacy Assay

All animal experiments were performed in compliance with the rules approved by the Biomedical Research Ethics Committee of Hebei University of Technology. BALB/c mice were randomly divided into five groups (n= 5 per group): PBS, HMPB@ZnP NPs, HMPB-GOx@ZnP NPs, HMPB-GOx@ZnP-DOX NPs, and HMPB-GOx@ZnP-DOX NPs + laser. The mean NP dose was equal to 6.27 mg/kg. Samples (200 μL) from the different groups were injected via the tail vein every other day. In the laser group, an 808 nm laser (1 W cm^{-2}, 5 min) was used to irradiate the tumor site after injection for 24 h (The irradiation distance is 10 cm). Body weight and tumor volume of the mice were recorded every two days. Tumors and major organs of the mice were collected at the experimental endpoint (10 d). Additionally, the collected organs (kidney, spleen, liver, lung, and heart) were subjected to tissue analysis using hematoxylin and eosin (H&E) staining, and all tumors were stained with H&E, terminal deoxynucleotidyl transferase dUTP nick end labeling (TUNEL), and Ki67 staining.

Results and Discussion

Synthesis and Characterization

The synthetic route to HMPB-GOx@ZnP-DOX NPs is shown in Scheme 1. The PB NPs were synthesized based on previous literatures.[41,42] Then, based on PB, HMPB was obtained via a hydrothermal method, which is a chemical etching process using hydrochloric acid as an etchant under the protection of PVP. After loading GOx into the existing macroporous structure of HMPB, the PAA-Zn solution, which was prepared by the acid-base neutralization reaction of ZnO and PAA, and IPA were successively added to form the HMPB-GOx@PAA-Zn NPs. Thereafter, by adding $NH_4H_2PO_4$ to react with the PAA-Zn layer, biodegradable ZnP shells were formed, which provided storage space for loading DOX, leading to the formation of the final HMPB-GOx@ZnP-DOX nanoplatforms for chemo/starvation/photothermal synergistic cancer therapy in vitro and in vivo.

The prepared PB NPs had a cubic shape, with an average size of 130 nm (Figure 1A). HMPB NPs were fabricated under the protection of PVP by etching the inner core of PB under strongly acidic conditions at high temperatures. The HMPB NPs changed from a cubic shape to an obvious cavity and abundant pore structure after hydrochloric acid etching (Figure 1B). The XRD results showed that the HMPB NPs maintained the crystalline form of PB (Figure 2A). According to the N_2 adsorption-desorption isotherm results, the pore size was approximately 30 nm, which further confirmed that the porosity of HMPB can provide an ideal space for the payload of GOx (Figure 2B). To avoid premature leakage of GOx and its easy degradation when exposed to physiological environments, ZnP was selected to coat the surface of the HMPB, which can only degrade under acidic conditions to protect GOx from deactivation and leakage before reaching

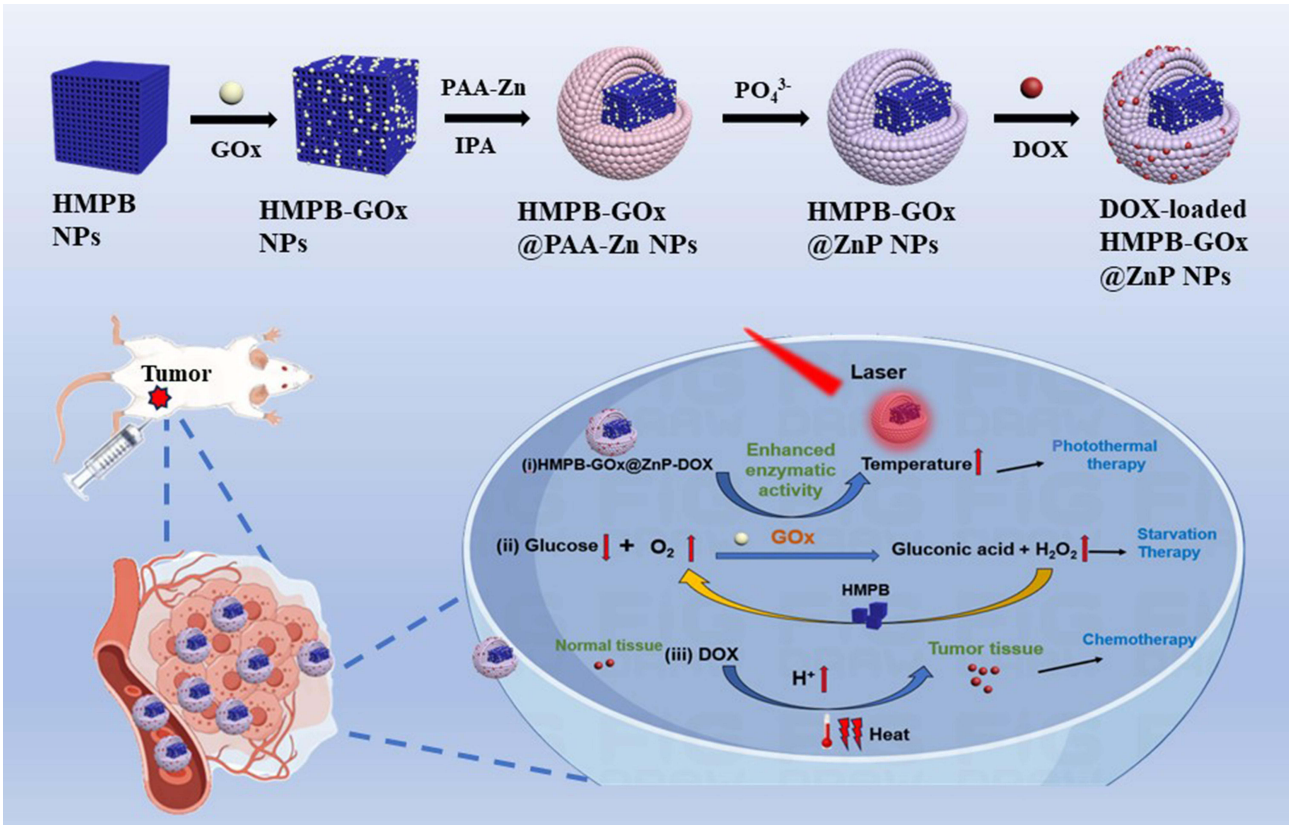

Scheme 1 Schematic illustration of preparing HMPB-GOx@ZnP-DOX NPs for the application of synergistic photothermal-augmented chemo-starvation therapy.

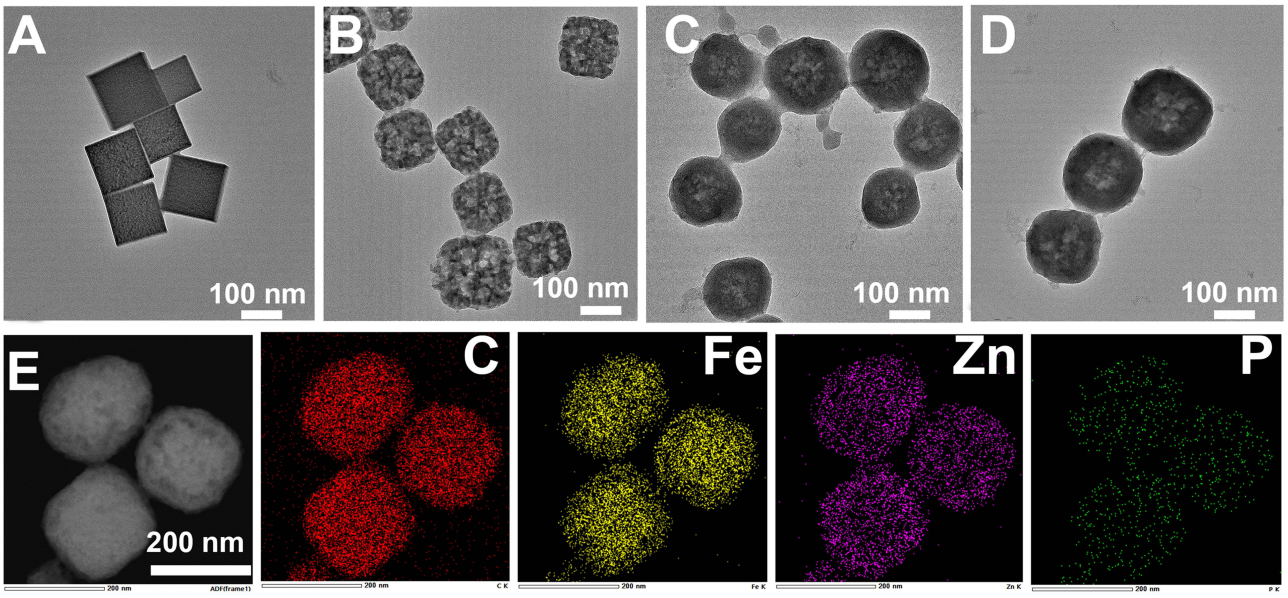

Figure 1 TEM images of (**A**) PB NPs; (**B**) HMPB NPs; (**C**) HMPB@ZnP NPs and (**D**) HMPB-GOx@ZnP-DOX NPs; (**E**) Element mapping images of HMPB@ZnP NPs.

the tumor sites. In this process, a PAA-Zn aqueous solution was first obtained through acid-base neutralization by adding ZnO powder to the PAA aqueous solution. Then, the PAA-Zn aqueous solution and IPA were successively added to the HMPB NPs loaded with GOx to form HMPB-GOx@PAA-Zn NPs because of the insolubility of PAA-Zn in the mixture

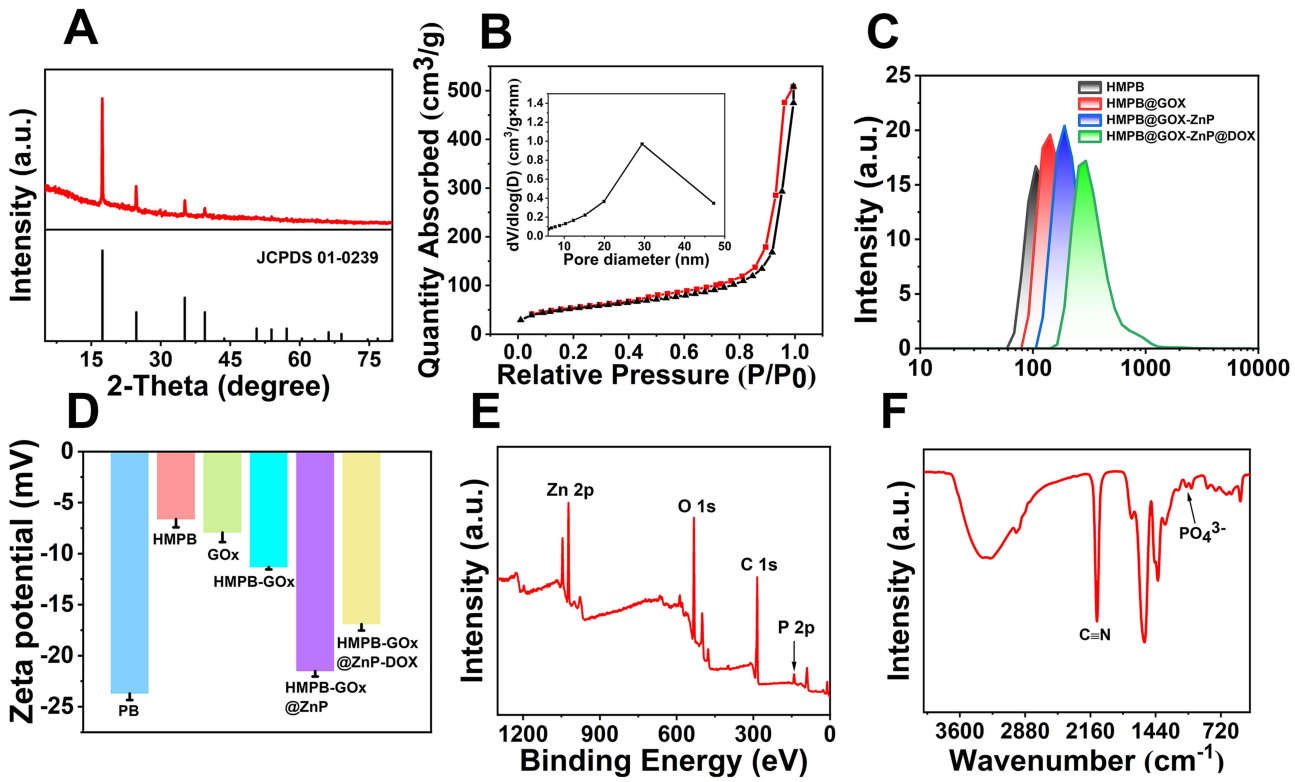

Figure 2 (**A**) XRD patterns of HMPB NPs; (**B**) N_2 adsorption/desorption isotherms of HMPB NPs (inset: pore size distribution); (**C**) Average sizes of HMPB, HMPB-GOx NPs, HMPB-GOx@ZnP NPs and HMPB-GOx@ZnP-DOX NPs; (**D**) Zeta potential of pure PB NPs, HMPB NPs, GOx, HMPB-GOx NPs HMPB-GOx@ZnP NPs and HMPB-GOx@ZnP-DOX NPs; (**E**) XPS of HMPB@ZnP NPs; (**F**) FTIR spectra of HMPB@ZnP NPs.

of water and IPA. Subsequently, $NH_4H_2PO_4$ was added as a phosphate anion source to react with the coated PAA-Zn layer and form a biodegradable ZnP shell on the surface of the HMPB NPs. Compared with HMPB NPs, the TEM and SEM images of HMPB@ZnP NPs exhibit that a significant coating layer is formed on the originally uneven surface (Figures 1C and S1). The TEM image of the HMPB-GOx@ZnP-DOX NPs were also observed, and no significant change was seen (Figure 1D). Furthermore, the hydrodynamic diameters steadily increased during the production procedure of HMPB-GOx@ZnP-DOX NPs (Figure 2C). The zeta potentials were also measured stepwise to confirm successful synthesis. As shown in Figure 2D, the initial zeta potential of HMPB was −6.61 mV, and the zeta potential became more negative after loading GOx. Furthermore, after coating ZnP on the HMPB, the zeta potential of the HMPB-GOx @ZnP NPs decreases to −21.5 mV, which is because the surface ZnP is synthesized from the PAA-Zn templates containing carboxyl groups. After loading DOX, the zeta potential of HMPB-GOx@ZnP-DOX NPs was increased to −16.9 mV, illustrating the successful fabrication of HMPB-GOx@ZnP-DOX NPs. To verify the structure, elemental mapping TEM images of the HMPB@ZnP NPs were obtained (Figure 1E). From these results, we can see that Fe, Zn, P, and C are consistent with the composition and distribution of the HMPB@ZnP NPs. Furthermore, the surface composition of the HMPB@ZnP NPs was investigated by X-ray photoelectron spectroscopy (XPS), which showed the existence of characteristic peaks of Zn, P, O, and C (Figure 2E). The presence of HMPB and ZnP was further detected by Fourier transform infrared (FTIR) spectroscopy, where the absorption peak at 2090 cm^{-1} came from the stretching vibration of C≡N in the HMPB NPs.[43] The absorption band at 1105 cm^{-1} was attributed to the characteristic stretching band of PO_4^{3-} ions (Figure 2F). [44] In addition, to evaluate the pore size of the ZnP shell, we used pure ZnP NPs as research object obtained by adding a phosphate anion source to pure PAA-Zn NPs templates in the absence of HMPB for N_2 adsorption-desorption tests (Figure S2). The result shows the pore diameter distribution centers at 6.1 nm, which is a suitable size that can avoid premature leakage of GOx while simultaneously offering another space for loading DOX. Thus, we used

the cavity of the HMPB core to load the macromolecule GOx and mesopores of the ZnP shell to load DOX, realizing the synergistic treatment of cancer with photothermally augmented chemo-starvation therapy.

Photothermal Effect

As shown in Figure 3A, the UV-vis absorption spectrum of HMPB-GOx@ZnP-DOX NPs showed apparent absorption in the range of 600–900 nm, and the absorption peak was centered at 735 nm, which inspired us to explore their potential for photothermal therapy of cancer. To assess photothermal conversion performance in vitro, a concentration-dependent increase in temperature was monitored (Figure 3B). The temperature of the HMPB-GOx@ZnP-DOX NPs solution (200 μg mL^{-1}) increases by 27.2 °C during 5 min of irradiation. Comparatively, the temperature of pure water only increases by 3.6 °C under the same conditions. Subsequently, the HMPB-GOx@ZnP-DOX solutions were exposed to 808 nm laser

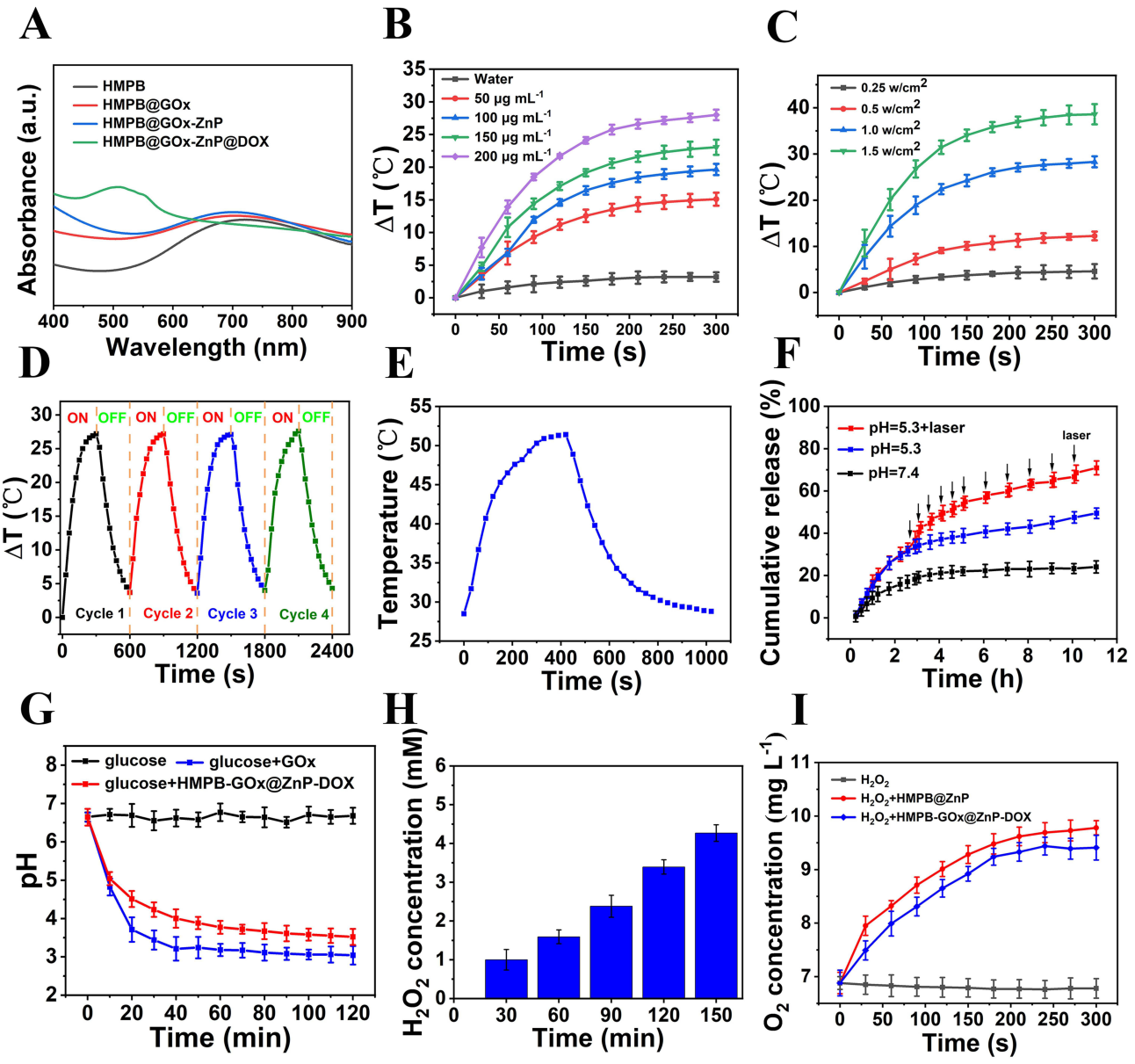

Figure 3 (**A**) UV-vis absorption spectra of HMPB, HMPB-GOx NPs, HMPB-GOx@ZnP NPs and HMPB-GOx@ZnP-DOX NPs; (**B**) Temperature elevation curves of HMPB-GOx@ZnP-DOX NPs with different concentrations under the 808 nm laser irradiation at 1W cm^{-2}; (**C**) Temperature elevation curves of HMPB-GOx@ZnP-DOX NPs (200 μg mL^{-1}) under different laser power; (**D**) Temperature changes of HMPB-GOx@ZnP-DOX NPs (200 μg mL^{-1}) during four cycles; (**E**) Temperature profile of HMPB-GOx @ZnP-DOX NPs under photothermal heating and natural cooling process; (**F**) Cumulative release curves of DOX under different conditions; (**G**) pH changes under different conditions; (**H**) The ability of HMPB-GOx@ZnP-DOX NPs to generate H_2O_2 at different time; (**I**) O_2 generation profiles of various samples in PBS (pH 7.4) at 37 °C.

irradiation at various power densities. Typically, the temperature of the solution containing HMPB-GOx@ZnP-DOX NPs (200 μg mL^{-1}) changes by 36.4 °C within 5 min at 1.5 W cm^{-2} (Figure 3C), which demonstrates that HMPB-GOx@ZnP-DOX NPs can efficiently convert NIR light into heat. The thermal images of HMPB-GOx@ZnP-DOX NPs irradiated with different concentrations and different laser powers are shown in Figure S3. To further explore the photothermal stability of the HMPB-GOx@ZnP-DOX NPs, the recycling temperature was changed under 808 nm laser irradiation for 5 min, followed by natural cooling to room temperature for four laser-on/off rounds cycles (Figure 3D). The photothermal performance of the HMPB-GOx@ZnP-DOX NPs showed no significant deterioration during cycling, suggesting that they are capable of effectively and durably producing abundant heat upon NIR irradiation. Based on the results of the time constant for heat transfer and maximum temperature, the photothermal-conversion efficiency (η) was calculated to be 24.67% (Figures 3E and S4). These results indicate that HMPB-GOx@ZnP-DOX NPs have the potential to be used as photothermal agents.

The Drug Loading and Release

To assess the drug loading capacity and controlled release behavior of HMPB-GOx@ZnP-DOX NPs, we calculated the drug loading content according to the characteristic absorbance of DOX (485 nm) and systematically analyzed the cumulative release percentage of DOX in pH- and NIR-responsive modes. The drug loading capacity and loading efficiency were calculated to be 31.9% and 97.5% based on the absorption value at the characteristic peak of DOX in the supernatant during the preparation of HMPB-GOx@ZnP-DOX NPs. Subsequently, the drug release behavior of HMPB-GOx@ZnP-DOX NPs with and without laser irradiation was tested in a simulated acidic tumor environment (pH 5.3) and a normal physiological environment (pH 7.4). As shown in Figure 3F, the amount of DOX released from the prepared HMPB-GOx@ZnP-DOX NPs was approximately 23.96% within 11 h at a pH of 7.4, and the release rate was relatively slow. In contrast, approximately 49.23% of DOX was released from HMPB-GOx@ZnP-DOX NPs at pH 5.3, confirming that HMPB-GOx@ZnP-DOX NPs had good acid-responsive drug-release properties, which is ascribed to the fact that ZnP can be degraded under acidic conditions. When HMPB-GOx@ZnP-DOX NPs were immersed in acidic conditions and treated with periodic laser irradiation, rapid release was observed, and the drug release amount increased to 70.91%. Obviously, DOX release from HMPB-GOx@ZnP-DOX NPs was significantly increased by NIR irradiation, and the photothermally enhanced release may have resulted from the accelerated motion of the drug molecule caused by the generated heat. Above all, HMPB-GOx@ZnP-DOX NPs can achieve controlled drug release under mild acidic conditions and NIR irradiation, providing the possibility of a multifunctional drug delivery nanoplatform for cancer combination therapy.

Enzyme Activity Assay and Oxygen Production Capacity

Given that GOx acts as a trigger point for starvation, detecting the enzymatic activity of HMPB-GOx@ZnP-DOX NPs is important for the success of the combination therapy in this study. To our knowledge, GOx, an endogenous oxidoreductase, can effectively convert glucose and O_2 within tumors into H_2O_2 and gluconic acid.[32] An increase in gluconic acid directly leads to a decrease in pH value. The generated H_2O_2 and decreased pH can be used as indicators to evaluate the enzymatic activity of GOx in the HMPB-GOx@ZnP-DOX NPs during glucose oxidation. As shown in Figure 3G, with the addition of HMPB-GOx@ZnP-DOX NPs to glucose, an obvious decrease in pH was observed. However, the pH of the pure glucose solution remains constant. Moreover, as illustrated in Figure 3H, the amount of generated H_2O_2 in the HMPB-GOx@ZnP-DOX solution, which can be calculated by the fitted standard curve of H_2O_2 concentration vs absorption (Figure S5), is increased with increasing reaction time. These results indicated that GOx loaded into the HMPB-GOx@ZnP-DOX NPs maintained their catalytic activity for glucose oxidation. PTT is engaged in the whole theranostic process, hence the enzymatic activity of HMPB-GOx@ZnP-DOX NPs should be investigated under NIR irradiation. In this experiment, the H_2O_2 concentration in the mixed solution of HMPB-GOx@ZnP-DOX NPs and glucose was irradiated by 808 nm laser with various power densities of 0, 0.25, 0.5, 1 and 1 0.5W cm^{-2} for 5 min, and the corresponded temperatures is 34 °C, 41 °C, 54 °C and 65 °C, respectively. It was shown that the enzymatic activity of HMPB-GOx@ZnP-DOX NPs increased with the rise of temperature, peaked between 41 °C and 54 °C, and subsequently decreased as the temperature further increases (Figure S6). It can be seen that the enzyme activity can be improved by

raising the temperature appropriately, but high temperature may cause enzyme inactivation. Moreover, because of the catalase-like activity of HMPB NPs, the tumor hypoxia problem can be alleviated by catalyzing H_2O_2 to generate O_2 to enhance the effectiveness of chemotherapy and starvation therapy.[45] This motivated us to investigate the catalase-like activity of the as-synthesized HMPB-GOx@ZnP-DOX NPs against H_2O_2. In this experiment, we used a dissolved-O_2 meter to monitor the change of O_2 concentration in the H_2O_2 solution at 37 °C (pH 7.4) with the addition of HMPB@ZnP NPs or HMPB-GOx@ZnP-DOX NPs over a period of 5 min (Figure 3I). In both the HMPB@ZnP+H_2O_2 and HMPB-GOx@ZnP-DOX+H_2O_2 groups, the O_2 concentration increased significantly with time, whereas the O_2 concentration in the pure H_2O_2 solution only retained an equilibrium level of only 7.8 mg/L, indicating that the HMPB@ZnP NPs and HMPB-GOx@ZnP-DOX NPs exhibited excellent O_2 production capacity owing to their catalase-like activity, which was beneficial to improve the effect of the combined therapy.

Cellular Uptake and Cell Cytotoxicity of HMPB-GOx@ZnP-DOX NPs

The cellular uptake of HepG-2 cells and drug delivery of these multifunctional NPs were investigated using CLSM, in which the red and blue fluorescence were derived from DOX and the nuclei were stained with DAPI. As shown in Figure 4A, the intrinsic red signal of DOX was clearly observed in HepG-2 cells after incubation with HMPB-GOX @ZnP-DOX NPs for 3h, implying that the HMPB-GOx@ZnP-DOX NPs could effectively enter the cells, and the loaded DOX could be released from the HMPB-GOx@ZnP-DOX NPs into the cytoplasm to exert their role in chemotherapy. Cell endocytosis was evaluated using quantitative flow cytometry (Figure 4B). After incubation with HMPB-GOX @ZnP-DOX NPs for 0.5, 1, 3, 5, and 6 h, fluorescence intensity was significantly enhanced. These results suggest that HMPB-GOx@ZnP-DOX NPs can effectively deliver therapeutic agents to tumor cells for cancer therapy.

Subsequently, the combined therapeutic efficacy of HMPB-GOX@ZnP-DOX NPs was assessed in HepG-2 cells through 3-(4,5-dimethyl-2-thiazolyl)2,5-diphenyltetrazolium bromide (MTT) assay. The HepG-2 cells were incubated with PBS, HMPB@ZnP NPs, HMPB-GOX@ZnP NPs, HMPB-GOX@ZnP-DOX NPs, or HMPB-GOX@ZnP-DOX NPs+laser. As shown in Figure S7, even when the concentration of HMPB@ZnP NPs reached 100 μg/mL, the survival rate of HepG-2 cells remained above 93%, illustrating the high biosafety of the blank material. In comparison, a slight decrease in cell viability was observed in the HMPB-GOX@ZnP NPs group, which was attributed to the weak effect of the starvation therapy alone. When the materials simultaneously delivered two therapeutic agents (HMPB-GOx@ZnP-DOX),

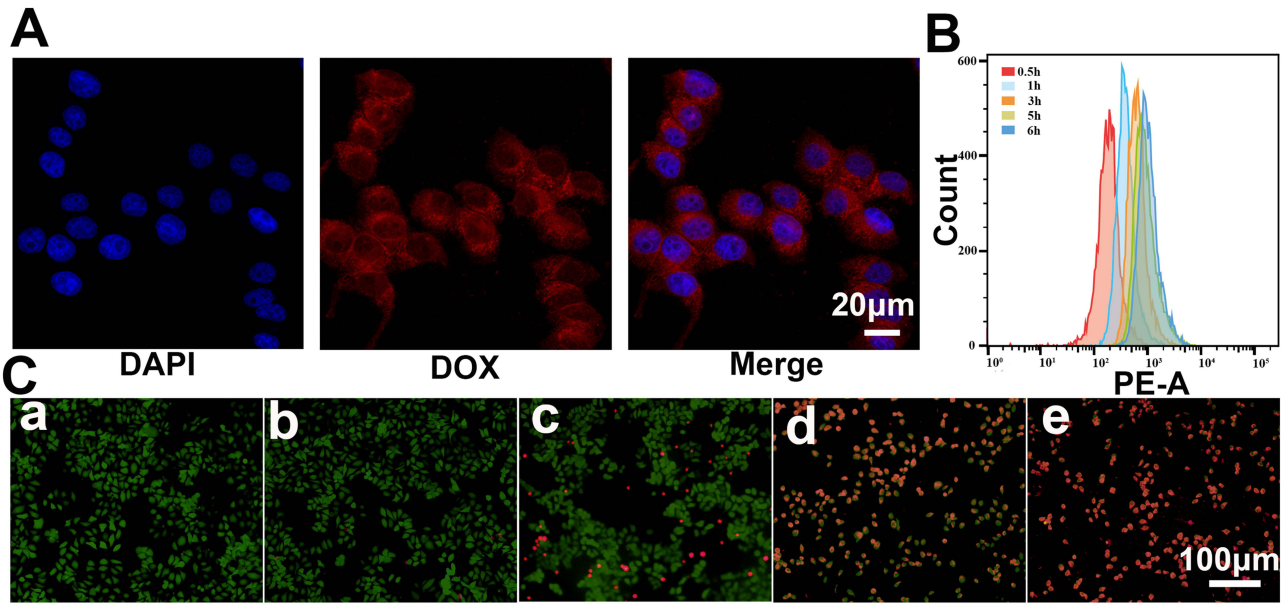

Figure 4 (**A**) CLSM images of cells incubated with HMPB-GOx@ZnP-DOX NPs for 3 h; (**B**) Flow cytometric results of HepG-2 cells incubated with HMPB-GOx@ZnP-DOX NPs for different time; (**C**) HepG-2 cells stained by Calcein-AM/PI after different treatments (a: control; b: HMPB@ZnP NPs; c: HMPB-GOx@ZnP NPs; d: HMPB-GOx@ZnP-DOX NPs; e: HMPB-GOx@ZnP-DOX NPs+laser).

cell viability decreased remarkably owing to the coordinated interaction between chemotherapy and starvation therapy. Notably, the HMPB-GOx@ZnP-DOX+laser group showed the highest mortality (79.06%) against cancer cells at all tested concentrations compared to the single starvation therapy (25.5%) or chemo/starvation combined therapy (62.60%), which benefits from the amplification effect of photothermal conversion on chemo- and starvation therapy. To further confirm the glucose consumption of HMPB-GOx@ZnP-DOX NPs in HepG-2 cells, the ATP levels were detected by an ATP assay kit. As shown in Figure S8, the result of HMPB-GOx@ZnP-DOX NPs group is comparable to the free GOx group, but displayed lower ATP levels compared to the HMPB@ZnP NPs group, which can be explained by the GOx loaded in the HMPB-GOx@ZnP-DOX NPs consuming large amount of glucose. Moreover, flow cytometry was used to quantitatively analyze the apoptosis ratios of HepG-2 cells under different treatments (Figure S9). The apoptosis percentage in control group is only 9.41%, while it increased to 26.64% and 51.76% in HMPB-GOx@ZnP NPs group and HMPB-GOx@ZnP-DOX NPs group, respectively. Most notably, the HMPB-GOx@ZnP-DOX NPs+ NIR group exhibited the most significantly apoptosis (72.5%). These results highlight the necessity and advantages of chemo/starvation/photothermal trimodal combined therapy.

To further visually observe the effect of the combination therapy, we co-stained the cells with calcein-AM and PI solutions and recorded the cell images using a fluorescence microscope. As shown in Figure 4C, the untreated cells grew well, and the cells incubated with HMPB@ZnP NPs showed only green fluorescence, suggesting that the blank material was not significantly toxic to cells. In comparison, the HMPB-GOx@ZnP NPs group showed a small portion of red fluorescence owing to the weak effect of the single starvation treatment. When the dual combination therapy of chemo- and starvation acted on the cells in the HMPB-GOx@ZnP-DOX group without laser irradiation, a higher ratio of red fluorescence was observed. When the cells incubated with HMPB-GOx@ZnP-DOX NPs were exposed to the 808 nm laser, it was evident that the cells were nearly dead and exhibited intense red fluorescence. Additionally, the toxic effect of HMPB@ZnP NPs on normal cells (293T cells) was tested in this work. When cultured with 293T cells even at concentrations of HMPB@ZnP NPs as high as 100 μg mL^{-1} for 24 h, there was no significant decrease in cell viability. These results show that the blank HMPB@ZnP NPs are high biocompatible and the prepared HMPB-GOx@ZnP-DOX NPs can serve as an effective anticancer nanoplatform for chemo/starvation/photothermal trimodal combined therapy (Figure S10).

In vivo Synergistic Therapy

The in vivo tumor suppression effect of HMPB-GOx@ZnP-DOX NPs was investigated in five groups of H-22 tumor-bearing mice: Control, HMPB@ZnP NPs, HMPB-GOX@ZnP NPs, HMPB-GOX@ZnP-DOX NPs, and HMPB-GOX @ZnP-DOX NPs + laser. To evaluate photothermal efficacy, mice injected with PBS and HMPB-GOX@ZnP-DOX NPs were monitored using an infrared camera to record changes in the tumor temperature. As revealed in Figure 5A, the tumor temperature in HMPB-GOX@ZnP-DOX NPs group increased obviously than the control group after 5 min irradiation, clarifying the photothermal prospect of HMPB-GOX@ZnP-DOX NPs in vivo. It was also demonstrated that the prepared drug-loaded HMPB-GOX@ZnP-DOX NPs could effectively aggregate at the tumor site due to the enhanced permeability and retention (EPR) effect.[46,47] To estimate the systemic toxicity of the materials and their therapeutic effect, the body weight and tumor volume of each mouse were measured every two days. From the body weight graph, it was found that the overall weight of mice in each group was relatively stable (Figure 5C). There was a slight decrease in the body weight of the HMPB-GOx@ZnP-DOX NPs and HMPB-GOx@ZnP-DOX NPs + laser groups compared to the control group, which can be attributed to the toxic effects on organisms with mild DOX leakage, which is negligible, indicating that the delivery system has high biosafety. According to the graph of tumor volume, the HMPB@ZnP-treated mice grew similarly to the PBS group, illustrating the biocompatibility of blank nanocarriers (Figure 5B). After loading GOx (HMPB-GOx@ZnP NPs group), a slight retardation in tumor growth was observed, suggesting that the effectiveness of a single starvation therapy is limited. In contrast, the anti-tumor effects of the HMPB-GOx@ZnP-DOX NPs group improved significantly, although suboptimal results were not achieved, proving that the simultaneous delivery of GOx and DOX as therapeutic agents can enhance treatment effectiveness to a certain extent. Notably, the HMPB-GOx @ZnP-DOX NPs +laser group showed the most effective tumor suppression (80.31%), which verified the potency of integrating chemo/starvation/photothermal trimodal therapy (Figure 5F).

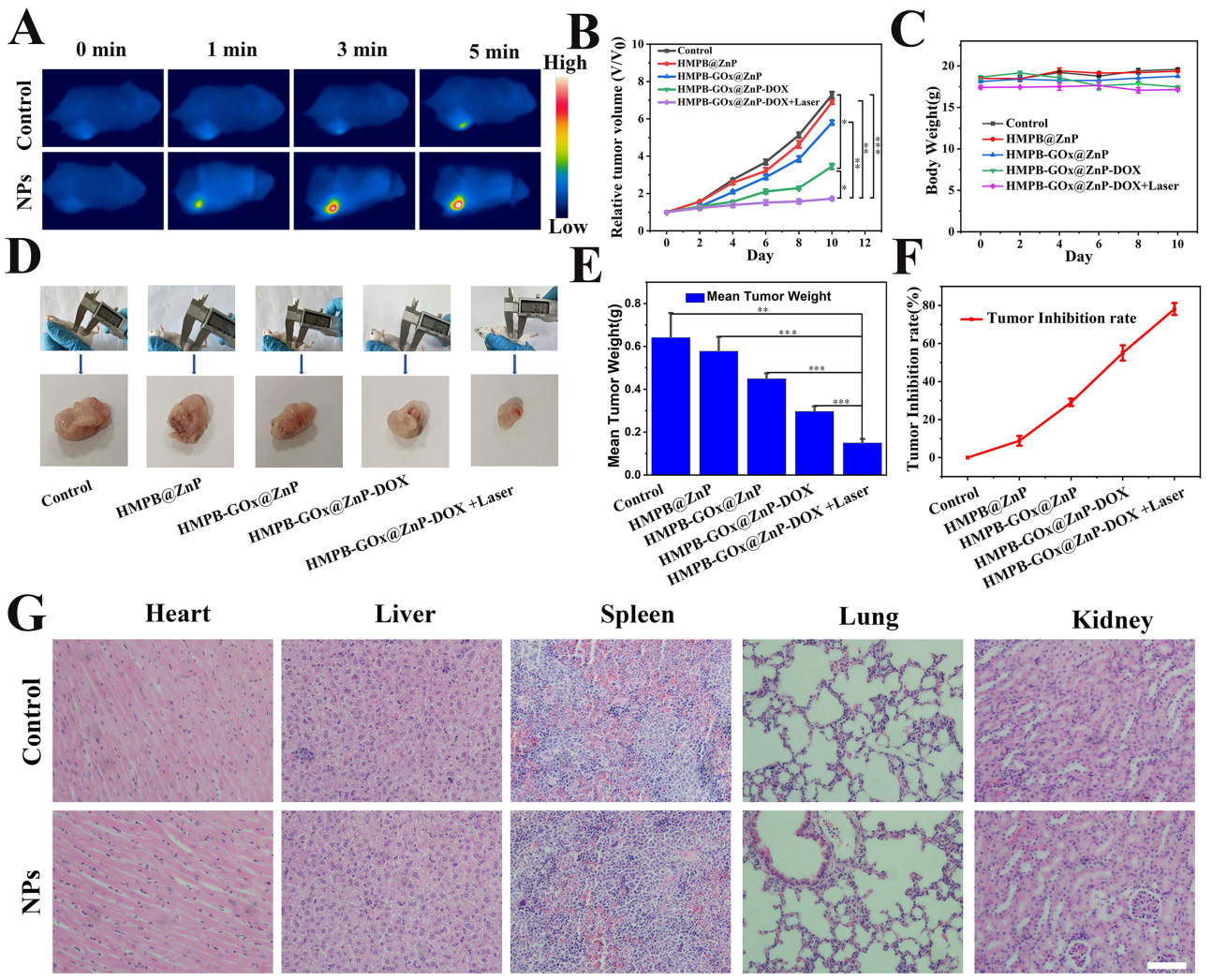

Figure 5 (**A**) Infrared thermal images of tumor-bearing mice after injection with HMPB-GOx@ZnP-DOX NPs and PBS under 808 nm laser irradiation. (**B**) Body weight and (**C**) tumor growth curves with various treatments. (**D**) The mean tumor weight and the tumor inhibition rate of each group every two days. (**E**) Photographs of tumors with various treatments. (**G**) H&E staining of the major organs after PBS and HMPB-GOx@ZnP-DOX NPs injection (Scale bar:50 μm).

Photographs and weights of resected tumors from tumor-bearing mice provided additional direct evidence for the therapeutic effect of the currently developed nanoplatforms (Figure 5D and E). To assess the biotoxicity of the blank delivery system, the main organs (the heart, liver, spleen, kidney, and lungs) of the control and HMPB@ZnP NPs groups were collected for histological analysis (Figure 5G). No evident pathological changes were observed in the HMPB@ZnP NP-treated groups compared with the PBS group, demonstrating the high biological safety of HMPB@ZnP NPs for therapeutic application.

To further assess the anti-tumor effect of HMPB-GOx@ZnP-DOX NPs, tumor slices from different treatment groups were analyzed using H&E, TUNEL, and Ki67 staining. As shown in Figure 6, H&E and TUNEL staining images showed that the nuclei reduction and cell necrosis in the treatment groups increased to various degrees compared with the control group, and the tumor treated with HMPB-GOx@ZnP-DOX NPs + laser exhibited the most severe tumor tissue damage. Ki67 immunohistochemistry assays showed that the active proliferation of tumor cells in the HMPB-GOx@ZnP-DOX NPs + laser group was the most inhibited in all groups, which is consistent with H&E and TUNEL staining. These results demonstrated that HMPB-GOx@ZnP-DOX NPs possess outstanding biocompatibility and can achieve efficient tumor suppression by photothermally augmented chemo-starvation therapy.

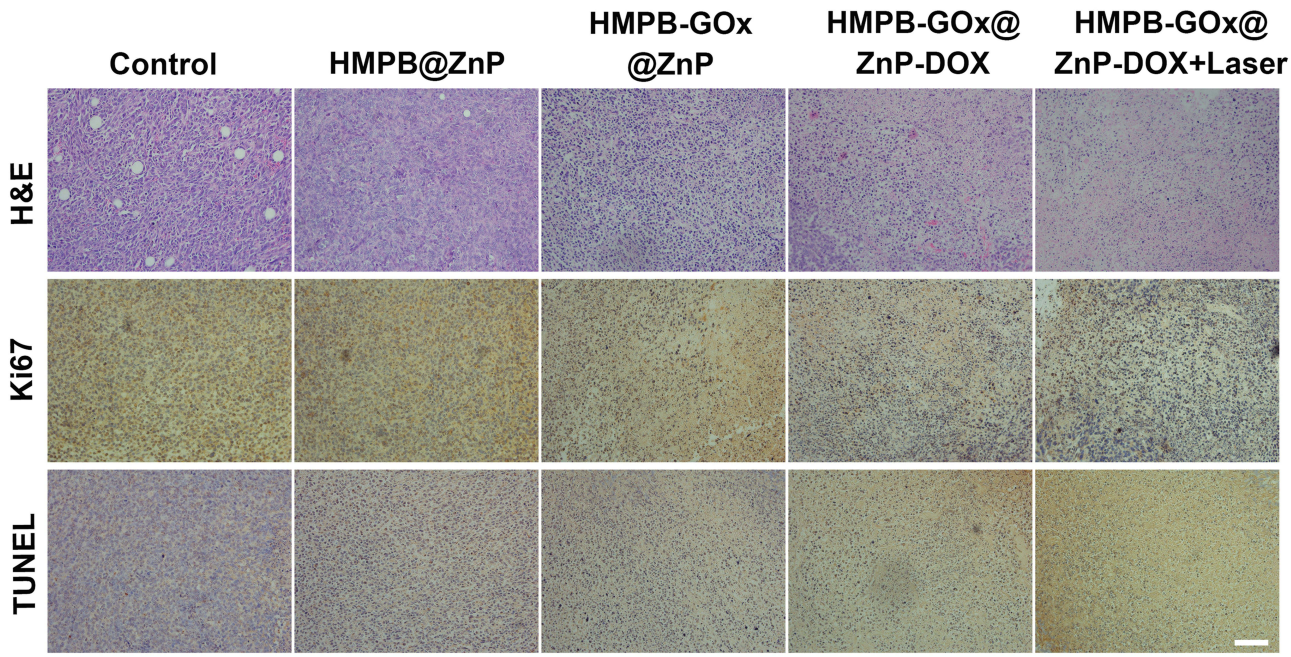

Figure 6 Microscopic pictures of the H&E, Ki67 and TUNEL-stained tumors with different treatments (scale bar:50 μm).

Conclusion

In this study, we created innovative nanoscale drug delivery systems (HMPB-GOx@ZnP-DOX NPs) capable of delivering GOx and DOX in different departments for photothermally enhanced chemical/starvation therapy. The coated ZnP shell achieved DOX loading and prevented premature leakage and degradation of GOx in the physiological environment. Meanwhile, owing to the pH-sensitivity of the ZnP shell, DOX and GOx can be released upon reaching acidic tumor sites. GOx can catalyze glucose oxidation to achieve starvation therapy, and more H_2O_2 is produced in this process, which can be further decomposed into O_2 under the catalase-like activity of HMPBs to relieve adverse conditions of anti-tumor. In addition, HMPB-GOx@ZnP-DOX NPs can ablate tumor cells through the photothermal conversion capability of the inner HMPB core, and the resulting hyperthermia can promote drug release and enzymatic activities to maximize the therapeutic effect. In vitro and in vivo experiments showed that HMPB-GOx@ZnP-DOX NPs presented high biosafety and significant tumor inhibition owing to photothermally augmented chemo-starvation therapy. Thus, this study provides new insights into the construction of multifunctional nanoplatforms for synergistic multimodal therapies.

Acknowledgments

Yuan Yuan and Mingyi Hou contributed equally to this work. We would like to thank the Natural Science Foundation of Hebei Province (B2021202036, B2021202048), Funded by Science and Technology Project of Hebei Education Department (BJ2021016), and the Project Supported by Hebei Technological Innovation Center of Chiral Medicine (ZXJJ20220203).

Disclosure

The authors report no conflicts of interest in this work.

References

1. Siegel RL, Miller KD, Wagle NS, et al. Cancer Statistics, 2023. *CA Cancer J Clin*. 2023;73(1):17–48. doi:10.3322/caac.21763
2. Chen QB, Shen MH, Ren XH, et al. Tumor-triggered targeting ammonium bicarbonate liposomes for tumor multimodal therapy. *J Mater Chem B*. 2022;10(27):5154–5164. doi:10.1039/D2TB00409G

3. Lu Y, Jia D, Ma X, et al. Reduction-responsive chemo-capsule-based prodrug nanogel for synergistic treatment of tumor chemotherapy. *ACS Appl Mater Interfaces*. 2021;13(7):8940–8951. doi:10.1021/acsami.0c21710
4. Wang JW, Chen QW, Luo GF, et al. A self-driven bioreactor based on bacterium metal organic framework biohybrids for boosting chemotherapy via cyclic lactate catabolism. *ACS Nano*. 2021;15(11):17870–17884. doi:10.1021/acsnano.1c06123
5. Li SL, Jiang P, Jiang FL, et al. Recent Advances in Nanomaterial-Based Nanoplatforms for Chemodynamic Cancer Therapy. *Adv Funct Mater*. 2021;31(22):2100243. doi:10.1002/adfm.202100243
6. Sritharan S, Sivalingam N. A comprehensive review on time-tested anticancer drug doxorubicin. *Life Sci*. 2021;278:119527. doi:10.1016/j.lfs.2021.119527
7. Rivankar S. An overview of doxorubicin formulations in cancer therapy. *J Cancer Res Ther*. 2014;10(4):853–858.
8. Dash BS, Lu YJ, Huang YS, et al. Chitosan-coated magnetic graphene oxide for targeted delivery of doxorubicin as a nanomedicine approach to treat glioblastoma. *Int J Biol Macromol*. 2024;260:129401. doi:10.1016/j.ijbiomac.2024.129401
9. Dash BS, Lu YJ, Pejrprim P, et al. Hyaluronic acid-modified, IR780-conjugated and doxorubicin-loaded reduced graphene oxide for targeted cancer chemo/photothermal/photodynamic therapy. *Adv Mater*. 2022;136:212764. doi:10.1016/j.bioadv.2022.212764
10. Dash BS, Lu YJ, Chen HA, et al. Magnetic and GRPR-targeted reduced graphene oxide/doxorubicin nanocomposite for dual-targeted chemo-photothermal cancer therapy. *Biomater Adv*. 2021;128:112311. doi:10.1016/j.msec.2021.112311
11. Ding CD, Tong L, Feng J, et al. Recent advances in stimuli-responsive release function drug delivery systems for tumor treatment. *Molecules*. 2016;21(12):1715. doi:10.3390/molecules21121715
12. Jia X, Zhang Y, Zou Y, et al. Dual intratumoral redox/enzyme-responsive NO-releasing nanomedicine for the specific, high-efficacy, and low-toxic cancer therapy. *Adv Mater*. 2018;30(30):1704490. doi:10.1002/adma.201704490
13. Luan T, Cheng L, Cheng J, et al. Tailored design of an ROS-responsive drug release platform for enhanced tumor therapy via "Sequential Induced Activation Processes". *ACS Appl Mater Interfaces*. 2019;11(29):25654–25663. doi:10.1021/acsami.9b01433
14. Yang K, Yu G, Yang Z, et al. Supramolecular polymerization-induced nanoassemblies for self-augmented cascade chemotherapy and chemodynamic therapy of tumor. *Angew Chem Int Ed*. 2021;60(32):17570–17578. doi:10.1002/anie.202103721
15. Yap TA, Parkes EE, Peng W, et al. Development of immunotherapy combination strategies in cancer. *Cancer Discov*. 2021;11(6):1368–1397. doi:10.1158/2159-8290.CD-20-1209
16. Han X, Gong C, Yang Q, et al. Biomimetic nano-drug delivery system: an emerging platform for promoting tumor treatment. *Int J Nanomed*. 2024;19:571–608. doi:10.2147/IJN.S442877
17. Yu S, Chen Z, Zeng X, et al. advances in nanomedicine for cancer starvation therapy. *Theranostics*. 2019;9(26):8026–8047. doi:10.7150/thno.38261
18. Song S, Wang D, Zhao K, et al. Donor-acceptor structured photothermal COFs for enhanced starvation therapy. *Chem Eng J*. 2022;442:135963. doi:10.1016/j.cej.2022.135963
19. Tu Z, Donskyi IS, Qiao H, et al. Graphene oxide-cyclic R10 peptide nuclear translocation nanoplatforms for the surmounting of multiple-drug resistance. *Adv Funct Mater*. 2020;30(35):2000933. doi:10.1002/adfm.202000933
20. Wu J, Zhang Y, Jiang K, et al. Enzyme-engineered conjugated polymer nanoplatform for activatable companion diagnostics and multistage augmented synergistic therapy. *Adv Mater*. 2022;34(18):2200062. doi:10.1002/adma.202200062
21. Fang C, Deng Z, Cao G, et al. Co-ferrocene MOF/glucose oxidase as cascade nanozyme for effective tumor therapy. *Adv Funct Mater*. 2020;30(16):1910085. doi:10.1002/adfm.201910085
22. Zhang W, Hu S, Yin JJ, et al. Prussian blue nanoparticles as multienzyme mimetics and reactive oxygen species scavengers. *J Am Chem Soc*. 2016;138(18):5860–5865. doi:10.1021/jacs.5b12070
23. Tian F, Zhong X, Zhao J, et al. Hybrid theranostic microbubbles for ultrasound/photoacoustic imaging guided starvation/low-temperature photothermal/hypoxia-activated synergistic cancer therapy. *J Mater Chem B*. 2021;9(45):9358–9369. doi:10.1039/D1TB01735G
24. Li J, Zhang W, Ji W, et al. Near infrared photothermal conversion materials: mechanism, preparation, and photothermal cancer therapy applications. *J Mater Chem B*. 2021;9(38):7909–7926. doi:10.1039/D1TB01310F
25. Liu S, Pan X, Liu H. Two-dimensional nanomaterials for photothermal therapy. *Angew Chem Int Ed*. 2020;59(15):5890–5900. doi:10.1002/anie.201911477
26. Jung HS, Verwilst P, Sharma A, et al. Organic molecule-based photothermal agents: an expanding photothermal therapy universe. *Chem Soc Rev*. 2018;47(7):2280–2297. doi:10.1039/C7CS00522A
27. Cheng Y, Wen C, Sun YQ, et al. Mixed-metal MOF-derived hollow porous nanocomposite for trimodality imaging guided reactive oxygen species-augmented synergistic therapy. *Adv Funct Mater*. 2021;31(37):2104378. doi:10.1002/adfm.202104378
28. Zhou L, Zhao J, Chen Y, et al. MoS_2-ALG-Fe/GOx hydrogel with Fenton catalytic activity for combined cancer photothermal, starvation, and chemodynamic therapy. *Colloid Surf B*. 2020;195:111243. doi:10.1016/j.colsurfb.2020.111243
29. Hu JJ, Liu MD, Gao F, et al. Photo-controlled liquid metal nanoparticle-enzyme for starvation/photothermal therapy of tumor by win-win cooperation. *Biomaterials*. 2019;217:119303. doi:10.1016/j.biomaterials.2019.119303
30. Xu Y, Bian J, Liu X, et al. Glucose-responsive enzymatic biomimetic nanodots for H_2O_2 self-supplied catalytic photothermal/chemodynamic anticancer therapy. *Acta Biomater*. 2023;172:441–453. doi:10.1016/j.actbio.2023.10.001
31. Cheng Y, Xia YD, Sun YQ, et al. "Three-in-One" nanozyme composite for augmented cascade catalytic tumor therapy. *Adv Mater*. 2024;36(8):2308033. doi:10.1002/adma.202308033
32. Yu H, Cheng Y, Wen C, et al. Triple cascade nanocatalyst with laser-activatable O_2 supply and photothermal enhancement for effective catalytic therapy against hypoxic tumor. *Biomaterials*. 2022;280:121308. doi:10.1016/j.biomaterials.2021.121308
33. Wang M, Chang M, Zheng P, et al. A noble AuPtAg-GOx nanozyme for synergistic tumor immunotherapy induced by starvation therapy-augmented mild photothermal therapy. *Adv Sci*. 2022;9(31):2202332. doi:10.1002/advs.202202332
34. Zhang L, Fu JM, Song LB, et al. Ultrasmall Bi/Cu coordination polymer combined with glucose oxidase for tumor enhanced chemodynamic therapy by starvation and photothermal treatment. *Adv Healthcare Mater*. 2023;13:2302264. doi:10.1002/adhm.202302264
35. Chen W, Zeng K, Liu H, et al. Cell membrane camouflaged hollow Prussian blue nanoparticles for synergistic photothermal-/chemotherapy of cancer. *Adv Funct Mater*. 2017;27(11):1605795. doi:10.1002/adfm.201605795
36. Chen Y, Li ZH, Hu JJ, et al. Remote-controlled multi-enzyme system for enhanced tumor therapy via dark/light relay catalysis. *Nanoscale Horiz*. 2020;5(2):283–293. doi:10.1039/C9NH00583H

37. Zhou J, Li M, Hou Y, et al. Engineering of a nanosized biocatalyst for combined tumor starvation and low-temperature photothermal therapy. *ACS Nano*. 2018;12(3):2858–2872. doi:10.1021/acsnano.8b00309
38. Liu J, Bu J, Bu W, et al. Real-time in vivo quantitative monitoring of drug release by dual-mode magnetic resonance and upconverted luminescence imaging. *Angew Chem Int Ed*. 2014;53(18):4551–4555. doi:10.1002/anie.201400900
39. Cai XJ, Gao W, Ma M, et al. A Prussian blue-based core-shell hollow-structured mesoporous nanoparticle as a smart theranostic agent with ultrahigh ph-responsive longitudinal relaxivity. *Adv Mater*. 2015;27(41):6382–6389. doi:10.1002/adma.201503381
40. Wang Z, Yu W, Yu N, et al. Construction of CuS@Fe-MOF nanoplatforms for MRI-guided synergistic photothermal-chemo therapy of tumors. *Chem Eng J*. 2020;400:125877. doi:10.1016/j.cej.2020.125877
41. Liu Y, Hong H, Xue J, et al. Near-Infrared radiation-assisted drug delivery nanoplatform to realize blood-brain barrier crossing and protection for parkinsonian therapy. *ACS Appl Mater Interfaces*. 2021;13(31):37746–37760. doi:10.1021/acsami.1c12675
42. Wang D, Zhou J, Shi R, et al. Biodegradable core-shell dual-metal-organic-frameworks nanotheranostic agent for multiple imaging guided combination cancer therapy. *Theranostics*. 2017;7(18):4605–4617. doi:10.7150/thno.20363
43. Ren C, Cheng Y, Li W, et al. Ultra-small Bi_2S_3 nanodot-doped reversible Fe(II/III)-based Hollow mesoporous Prussian blue nanocubes for amplified tumor oxidative stress-augmented photo-/radiotherapy. *Biomater Sci*. 2020;8(7):1981–1995. doi:10.1039/C9BM02014D
44. Wang C, Zhang L, Li S, et al. A designed synthesis of multifunctional Fe_3O_4@Carbon/Zinc phosphate nanoparticles for simultaneous imaging and synergic chemo-photothermal cancer therapy. *J Mater Chem B*. 2016;4(35):5809–5813. doi:10.1039/C6TB01669C
45. Zhou T, Lian X, Wang P, et al. A hepatocellular carcinoma targeting nanostrategy with hypoxia-ameliorating and photothermal abilities that, combined with immunotherapy, inhibits metastasis and recurrence. *ACS Nano*. 2020;14(10):12679–12696. doi:10.1021/acsnano.0c01453
46. Ikeda-Imafuku M, Wang LL-W, Rodrigues D, et al. Strategies to improve the EPR effect: a mechanistic perspective and clinical translation. *J Control Release*. 2022;345:512–536. doi:10.1016/j.jconrel.2022.03.043
47. Mohammadzadeh V, Rahiman N, Hosseinikhah SM, et al. Novel EPR-enhanced strategies for targeted drug delivery in pancreatic cancer: an update. *J Drug Del Sci Tech*. 2022;73:103459. doi:10.1016/j.jddst.2022.103459